Strange Sea Polarization in the Nucleon

by

Felix Dashevskiy

Submitted to the Department of Physics
in partial fulfillment of the requirements for the degree of

Bachelor of Science in Physics

at the

MASSACHUSETTS INSTITUTE OF TECHNOLOGY

June 1999

Author ....
Department of Physics
May 7, 1999

Certified by ....
Richard Milner
Associate Professor of Physics
Thesis Supervisor

Accepted by ....
Professor David E. Pritchard
Undergraduate Thesis Coordinator

Strange Sea Polarization in the Nucleon

by

Felix Dashevskiy

Submitted to the Department of Physics
on May 7, 1999, in partial fulfillment of the
requirements for the degree of
Bachelor of Science in Physics

Abstract

This thesis decribes an analysis technique which can be used to extract the Δs contribution to the nucleon spin from data obtained using the HERMES experiment at DESY, Hamburg, Germany. The results of the analysis of the 1996 and 1997 polarized hydrogen target data are presented. In the simplest interpretation, these results suggest a large positive polarization in the strange sea of the nucleon. Studies of the results and other possible interpretations are presented as well.

Thesis Supervisor: Richard Milner
Title: Associate Professor of Physics

Acknowledgments

This thesis is a culmination of several years of work and would not have been possible without help from many people. I wish to thank some of them here.

I wish to express my gratitude to Professor Richard Milner, my thesis supervisor, for his encouragement and guidance throughout my time at MIT Lab for Nuclear Science. I wish to thank him for providing me with the opportunity to do cutting edge research with the HERMES experiment. It has been an honor to work in his group. I have learned a great deal working on this project, and my undergraduate experience would not be complete without it. Professor Milner has also given me a chance to visit DESY in Germany, an experience which taught me not to travel without a visa.

My deepest thanks go to Bryan Tipton, who taught me everything I know about programming, strange quarks, HERMES, LNS, and ballroom dancing. This work would not be possible without his help and advice. He has an amazing grasp of the current particle physics (as well as any other physics I know of) and I thank him for putting so much time into teaching me some of it. I want to wish Bryan luck on his upcoming PhD thesis defense and his future endeavors.

I also want to thank all the graduate students up in the 5th floor office of Building 26: Mark Sutter, Jeff Martin, Taeksu Shin, Nik Gregory and Kevin McIlhany (although he's technically not on the 5th floor and not a graduate student, but nobody is perfect). Our discussions of this work, HERMES, physics, and meaning of life were an integral part of my LNS experience. Whether in the office, in Toscaninis or "offsite," I always enjoyed their company and insights. I also want to thank Arthur Mateos for hiring me and helping me start up at LNS. I only regret that I didn't get to know him better. I wish him luck with his career.

Finally, I wish to thank the people who have made my MIT experience fun, challenging, rewarding and unique. My undergraduate advisor and teacher, Professor Richard Yamamoto, has taught me the basics of experimental techniques and guided me through my MIT career. John Richardson and Karolen Paularena, with whom I co-authored my first published paper, I thank for teaching me the ropes of research science. I want to thank Professor Robert Jaffe, who taught my Quantum Physics III course, for making us learn LaTeX. I am very grateful to MIT for its Undergraduate Research Opportunities Program which makes it possible for undergraduates to exprience real science and work beside world's greatest minds.

I want to thank my brothers at old ΣΦΕ, without whom I would have never made it through this place. And above all, I thank my family for providing the support and love that we all need so much.

Contents

List of Figures

List of Tables

Chapter 1

Introduction

Electromagnetic scattering has been one of the most useful tools in the study of the structure of matter. The discovery of the atomic nucleus by Rutherford in 1909 is one of the first examples of the successes of scattering experiments. As the energies of particle accelerators have increased, we have been able to probe deeper and deeper into the subatomic world. By the end of the 1960's it was discovered that the unpolarized structure functions of the nucleon are largely independent of the momentum transfer Q^2 at high energies. This "scaling behavior" implies that nucleons are made up of pointlike constituents called partons. The partons were identified as quarks, which were the hypothetical constituent particles invented in order to classify the observed spectrum of baryons and mesons[9].

There are six known quark flavors: up, down, strange, charmed, bottom and top (symbolically, u, d, s, c, b, and t). Only three flavors are of significance in the nucleon, u, d, and s. The momentum carried by these partons makes up only about 50% of the momentum of the nucleon. With the help of quantum chromodynamics (QCD) the remaining momentum has been identified with neutral vector bosons which carry the force exchanged between quarks, called gluons[9]. Similarly, the constituent quarks were found to carry only about one third of the total nucleon spin[9]. Electromagnetic scattering has since been used to attempt to solve this spin puzzle. The topic of this thesis is the determination of the strange quark contribution to the nucleon spin using the data obtained from deep inelastic scattering experiments.

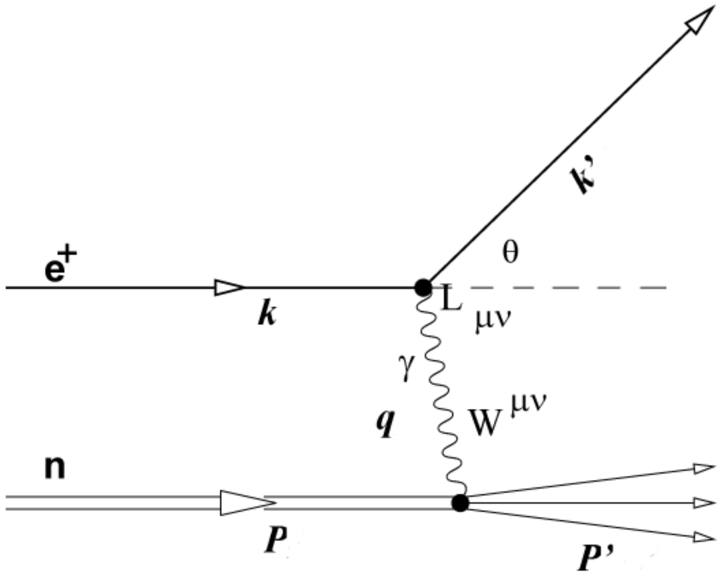

Figure 1-1: Basic Feynman diagram of a DIS event.

1.1 Basic Framework

The simple assignment of the masses to constituent quarks can be used to successfully derive the masses of hadrons[9]. Similarly, simple assignment of anomalous magnetic moments to the constituent quarks was used to explain the magnetic moment of the nucleon. In 1987, however, experiments by the EMC collaboration showed that only about 30% of the nucleon spin was carried by the quarks[2]. This result immediately aroused immense interest in the spin structure of the nucleon. The internal dynamic spin structure can be studied by scattering polarized beams off polarized targets. The HERMES experiment was designed specifically for this purpose. It is used to study deep inelastic scattering of leptons off nucleons.

1.1.1 Deep Inelastic Scattering

Deep inelastic scattering (DIS) is the study of lepton-hadron scattering in the limit of high momentum transfer. To lowest order in quantum electrodynamics, such scattering is described by an exchange of a virtual photon[2]. The basic Feynman diagram is shown in Figure 1-1[12]. Both the target and the beam are polarized, and the scattering cross-section is dependent on these spins, allowing the study of the spin structure of the target[9] (see Section 1.1.2 for more details). Inclusive measurements have produced a wealth of data, but the HERMES experiment specializes in the semi-inclusive studies which measure the final hadronic state. This allows for an investigation of the flavor dependence of the structure functions, thus creating a possibility of uncovering the strange quark contribution to the nucleon spin, which is the topic of this thesis.

1.1.2 The Quark Parton Model

The simplest model of nucleon structure is the static quark parton model. This model, originally developed by Feynman[5] and Bjørken and Paschos[1], assumes that nucleon constituents, partons, have certain momentum distributions, expressed as a fraction x_{Bj} of the total nucleon momentum[9]. It is these partons that leptons scatter off in DIS. Once partons were discovered, they were identified with quarks, which until then were simply convenient mathematical quantities used to classify the multitude of hadrons produced in accelerators. Protons and neutrons consist of three valence quarks. Only the two lightest quarks, u and d, are found among the valence quarks of nucleons. The quarks are spin-$\frac{1}{2}$ particles, and carry fractional charge. The u quarks have $+\frac{2}{3}e$ charge, while d and s quarks have $-\frac{1}{3}e$ charge (e is the electron charge)[2].

1.1.3 Quantum Chromodynamics

The shortcomings of the naive quark model have led to a development of a more advanced theory. Quantum chromodynamics (QCD) is the non-Abelian gauge theory which uses the "color" quantum number of quarks as the source of color force fields. The field bosons of QCD are called gluons[2]. Gluons are massless, spin-1 particles which themselves carry "color" charge and can decompose into quark-antiquark pairs. QCD has been extremely successful in describing many experimental results. In principle, QCD can be used to predict the quark wavefunctions inside the nucleus. However, such calculations are extremely difficult and not yet far enough advanced[2]. The valence quarks carry all of the charge in the nucleon, but only parts of the momentum and spin. Much of the momentum is carried by the gluons[9]. Virtual pairs of quarks and anti-quarks are dynamically generated in the nucleons, due to the Heisenberg Uncertainty Principle and related quantum fluctuations. These "sea quarks" are not confined to the lightest quarks, but the contributions of c, b and t flavors are negligible. It is generally assumed that the sea quarks do not carry much momentum and are thus abundant at low momentum fraction. The sea, however, may be significantly contributing to the spin of the nucleon.

1.1.4 Kinematics of DIS

The important variables of the DIS process are the four-momenta of the incoming lepton (k), the outgoing lepton (k'), the nucleon (p), the final hadronic state (p'), and the virtual photon ($q = k - k'$) (see Figure 1-1). The following Lorentz invariants are defined:

$$s = (k + p)^2 \tag{1.1}$$

$$Q^2 = -q^2 = -(k - k')^2 > 0 \tag{1.2}$$

$$\nu = \frac{p \cdot q}{M} \tag{1.3}$$

$$W^2 = p'^2 = M^2 + 2M\nu - Q^2 \tag{1.4}$$

where M is the mass of the nucleon. The mass of the lepton can be neglected. In the laboratory frame of a fixed target experiment where the energies of the lepton before and after are E and E' respectively and θ is the scattering angle, the Lorentz invariants can be calculated as

$$Q^2 = 4EE' \sin^2 \frac{\theta}{2} \tag{1.5}$$

$$\nu = E - E' \tag{1.6}$$

where ν is the energy transfer of the virtual photon to the nucleon and Q^2 is the invariant mass of the virtual photon which defines the resolution of the scattering process. The dimensionless scaling variables x_{Bj} and y are defined as

$$x_{Bj} = \frac{Q^2}{2p \cdot q} = \frac{Q^2}{2M\nu} \tag{1.7}$$

$$y = \frac{p \cdot q}{p \cdot k} = \frac{\nu}{E}. \tag{1.8}$$

x_{Bj} represents the momentum fraction carried by a quark[2]. Since there are three valence quarks, each one is expected to have average x_{Bj} peak around $\frac{1}{3}$. Since sea quarks do not carry much momentum, they have lower average x_{Bj}. The kinematically allowed ranges for these variables are

$$0 < x_{Bj} < 1 \tag{1.9}$$

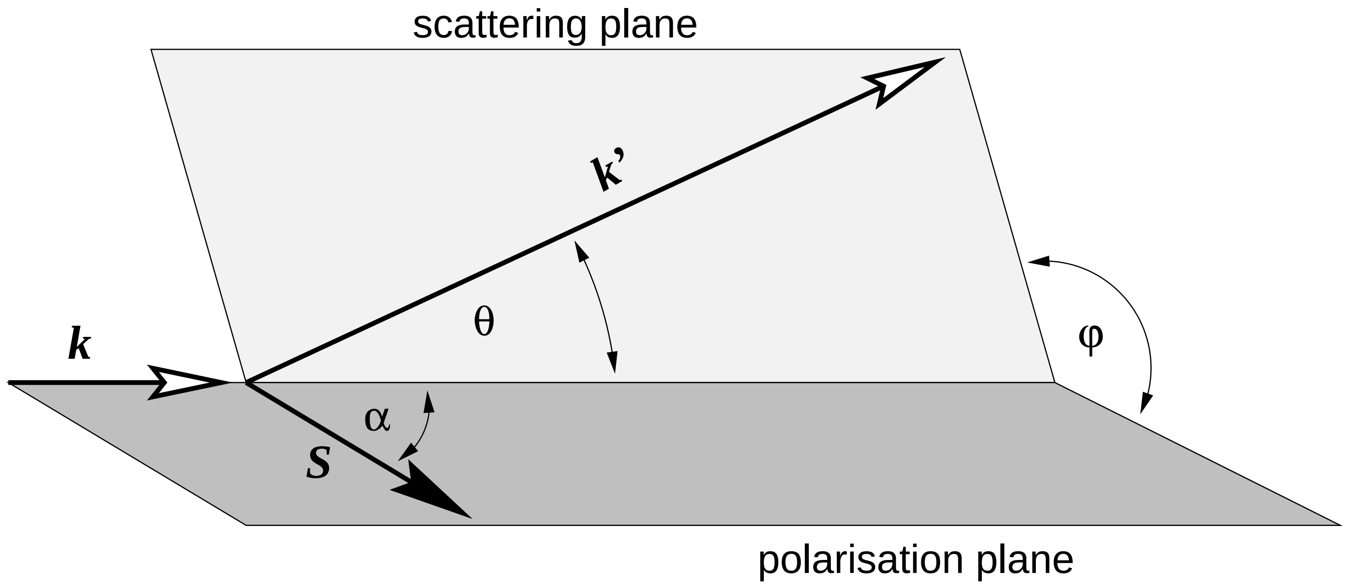

Figure 1-2: Definition of angles in DIS.

$$0 < y < \frac{1}{1 + x_{Bj}M/2E} < 1. \tag{1.10}$$

For a fixed beam energy E, the kinematics of DIS are completely determined by two variables, E' and θ. This experimentally measured pair is usually converted into the pair (x_{Bj}, Q^2) or (ν, Q^2)[2].

In the case of transversly polarized targets there is a third degree of freedom in the angle ϕ between the target polarization direction and the scattering plane of the lepton as seen in Figure 1-2[12]. α is the angle of the target polarization with respect to the beam direction[2].

In semi-inclusive measurements, another scaling variable z is introduced. It is Lorentz invariant and relates the energy E_h of the hadron to the maximum available energy ν in the lab frame[2]:

$$z = \frac{p \cdot p_h}{p \cdot q} = \frac{E_h}{\nu} \tag{1.11}$$

$$0 < z < 1. \tag{1.12}$$

1.1.5 Cross-Sections

The Unpolarized Cross-Section

The DIS cross-section can be expressed in terms of the leptonic and hadronic tensors, $L^{\mu\nu}$ and $W_{\mu\nu}$:

$$\frac{d^2\sigma}{d\Omega dE'} = \frac{\alpha^2 E'}{Q^4 E} L^{\mu\nu} W_{\mu\nu} \tag{1.13}$$

where $\alpha = 1/137.04$ is the fine-structure constant. The leptonic tensor is calculated from the spinors u according to the Feynman rules:

$$L^{\mu\nu} = \sum_{s_l'} (\bar{u}(k', s_l')\gamma^\mu u(k, s_l)) \cdot (\bar{u}(k, s_l)\gamma^\nu u(k', s_l')). \tag{1.14}$$

If the beam and target are unpolarized, the initial spins s_l are averaged and the leptonic tensor becomes

$$L^{\mu\nu} = 2[k^{\mu\prime} k^\nu + k^\mu k^{\nu\prime} + (m_e^2 - k \cdot k')g^{\mu\nu}] \tag{1.15}$$

where m_e is the electron mass and can be neglected. $g^{\mu\nu}$ is the metric tensor. The hadronic tensor reflects the structure of the nucleon and can be reduced to two real functions, W_1 and W_2:

$$W_{\mu\nu} = W_1(Q^2, \nu)(-g_{\mu\nu} + \frac{q_\mu q_\nu}{q^2}) + \frac{W_2(Q^2, \nu)}{M^2}(p_\mu - \frac{p \cdot q}{q^2} q_\mu)(p_\nu - \frac{p \cdot q}{q^2} q_\nu). \tag{1.16}$$

If we introduce dimensionless structure functions

$$F_1(x_{Bj}, Q^2) = M W_1(Q^2, \nu) \tag{1.17}$$

$$F_2(x_{Bj}, Q^2) = \nu W_2(Q^2, \nu) \tag{1.18}$$

the unpolarized cross-section becomes[2]

$$\frac{d^2\sigma}{d\Omega dE'} = \frac{4\pi\alpha^2}{Q^4} \cdot [F_1(x_{Bj}, Q^2) \cdot y^2 + \frac{F_2(x_{Bj}, Q^2)}{x_{Bj}} \cdot (1 - y - \frac{M x_{Bj} y}{2E})]. \tag{1.19}$$

The Polarized Cross-Section

The polarized cross-section contains additional terms in order to take into account the azimuthal angle ϕ:

$$\frac{d^3\sigma}{d\cos\theta d\phi dE'} = \frac{\alpha^2 E'}{Q^4 E} L^{\mu\nu} W_{\mu\nu} \tag{1.20}$$

The leptonic tensor in Equation 1.14 becomes

$$L^{\mu\nu} = 2[k^{\mu\prime} k^{\nu} + k^{\mu} k^{\nu\prime} - k \cdot k' g^{\mu\nu} - i\epsilon^{\mu\nu\alpha\beta} q_{\alpha} s_{l\beta}] \tag{1.21}$$

where $s_{l\beta}$ is the spin four-vector of the incoming lepton and $\epsilon^{\mu\nu\alpha\beta}$ is the totally anti-symmetric Levi-Civita tensor. The general form of the hadronic tensor in the polarized case is

$$\begin{aligned} W_{\mu\nu} = W_1(Q^2,\nu)(-g_{\mu\nu} + \frac{q_\mu q_\nu}{q^2}) \\ + \frac{W_2(Q^2,\nu)}{M^2}(p_\mu - \frac{p\cdot q}{q^2} q_\mu)(p_\nu - \frac{p\cdot q}{q^2} q_\nu) \\ + G_1(Q^2,\nu) M i\epsilon_{\mu\nu\lambda\sigma} q^\lambda s_h^\sigma \\ + \frac{G_2(Q^2,\nu)}{M} i\epsilon_{\mu\nu\lambda\sigma} q^\lambda (p\cdot q s_h^\sigma - s_h \cdot q p^\sigma) \end{aligned} \tag{1.22}$$

where s_h is the axial polarization vector of a spin-1/2 target. Because of the symmetries of the leptonic and hadronic tensors, the polarization assymetry of the cross-section is completely determined by the anti-symmetric part of $W_{\mu\nu}$.

In analogy to the unpolarized case, two dimensionless spin structure functions are introduced:

$$g_1(x_{Bj}, Q^2) = M^2 \nu G_1(Q^2,\nu) \tag{1.23}$$

$$g_2(x_{Bj}, Q^2) = M \nu^2 G_2(Q^2,\nu) \tag{1.24}$$

With these definitions, the spin-dependent part of the polarized DIS cross-section is given by

$$\begin{aligned} \frac{d^3(\sigma(\alpha) - \sigma(\pi+\alpha))}{dx dy d\phi} = \frac{e^4}{4\pi^2 Q^2}[\cos\alpha([1 - \frac{y}{2} - \frac{y^2}{4}\gamma^2] g_1(x_{Bj}, Q^2) - \frac{y}{2}\gamma^2 g_2(x_{Bj}, Q^2)) \\ - \sin\alpha\cos\phi\sqrt{\gamma^2[1 - y - \frac{y^2}{4}\gamma^2]}(\frac{y}{2} g_1(x_{Bj}, Q^2) + g_2(x_{Bj}, Q^2))] \end{aligned} \tag{1.25}$$

where γ is defined as $\gamma = \sqrt{Q^2}/\nu$ and α was defined in Section 1.1.3 (See Figure 1-2)[2].

Cross-Section Asymmetries

The experimentally measured asymmetries $A_{||}$ and $A_{\perp}$ are obtained by reversing the spin of the longitudinally and transversely polarized target:

$$A_{||} = \frac{\sigma^{\uparrow\downarrow} - \sigma^{\uparrow\uparrow}}{\sigma^{\uparrow\downarrow} + \sigma^{\uparrow\uparrow}} \tag{1.26}$$

$$A_{\perp} = \frac{\sigma^{\uparrow\rightarrow} - \sigma^{\uparrow\leftarrow}}{\sigma^{\uparrow\rightarrow} + \sigma^{\uparrow\leftarrow}}. \tag{1.27}$$

These cross-section asymmetries are related to the asymmetries of the virtual photon by

$$A_{||} = \mathcal{D} \cdot (A_1 + \eta \cdot A_2) \tag{1.28}$$

$$A_{\perp} = d \cdot (A_2 - \xi \cdot A_1). \tag{1.29}$$

The kinematic factors are defined as follows:

$$\mathcal{D} = \frac{y(2-y)}{y^2 + 2(1-y)(1+R)} \tag{1.30}$$

$$\eta = \frac{2\gamma(1-y)}{(2-y)} \tag{1.31}$$

$$d = \mathcal{D}\sqrt{\frac{2\epsilon}{1+\epsilon}} \tag{1.32}$$

$$\xi = \eta\frac{1+\epsilon}{2\epsilon} \tag{1.33}$$

where ϵ is the degree of tranverse polarization of the virtual photon and $R(x_{Bj}, Q^2)$ is the ratio of cross-sections for longitudinally and tranversely polarized photons. $\mathcal{D}$ is the depolarization factor, measuring the depolarization of the photon relative to the polarization of the scattered lepton[2].

1.1.6 Quark Distributions

In the quark parton model, the DIS process may be interpreted as an incoherent superposition of elastic scattering off partons. Using the kinematics of elastic scattering, it is possible to relate the structure functions to quark distributions, $q_f^{+(-)}(x_{Bj})$, which are the probability of finding a quark of flavor f with helicity anti-parallel (parallel) to nuclear spin with the momentum fraction x_{Bj} (x from now on)[2]. The structure functions can be expressed as

$$F_1(x,Q^2) = \sum_f \frac{e_f^2}{2}(q_f^+(x) + q_f^-(x)) \tag{1.34}$$

$$F_2(x,Q^2) = x\sum_f e_f^2(q_f^+(x) + q_f^-(x)) \tag{1.35}$$

$$g_1(x,Q^2) = \sum_f \frac{e_f^2}{2}(q_f^+(x) - q_f^-(x)) \tag{1.36}$$

$$g_2(x,Q^2) = 0. \tag{1.37}$$

The sums above are over all quark flavors contributing to the structure of the nucleon at a given momentum transfer. e_f is the charge factor for the flavor f. In a simple parton model, the structure functions are completely independent of Q^2[2].

The Unpolarized Quark Distributions

The unpolarized structure functions are determined by the unpolarized quark distributions, $q_f(x) = \frac{1}{2}(q_f^+(x) + q_f^-(x))$. From Equations 1.34 and 1.35 it follows that

$$F_1(x) = 2xF_2(x). \tag{1.38}$$

This is known as Callan-Gross relation[2]. The nucleon structure functions are

$$F_2^p(x) = x(\frac{4}{9}u(x) + \frac{1}{9}d(x) + \frac{1}{9}s(x) + \frac{4}{9}\bar{u}(x) + \frac{1}{9}\bar{d}(x) + \frac{1}{9}\bar{s}(x)) \tag{1.39}$$

$$F_2^n(x) = x(\frac{1}{9}u(x) + \frac{4}{9}d(x) + \frac{1}{9}s(x) + \frac{1}{9}\bar{u}(x) + \frac{4}{9}\bar{d}(x) + \frac{1}{9}\bar{s}(x)) \tag{1.40}$$

for proton and neutron respectively. The SU(2) isospin symmetry has been assumed and in the case of the neutron, $u(x)$ is the distribution of the down quark, while $d(x)$ is the distribution of the up quark[2].

The Polarized Quark Distributions

While the structure function $F_2(x)$ is related to unpolarized quark distributions, the function $g_1(x)$ has been shown to be related to the spin distributions $\Delta q_f(x)$ of the quarks:

$$\Delta q_f(x) = \frac{1}{2}(q_f^+(x) - q_f^-(x)). \tag{1.41}$$

Explicitly, the spin structure function for the proton is

$$g_1^p(x) = \frac{1}{2}(\frac{4}{9}\Delta u(x) + \frac{1}{9}\Delta d(x) + \frac{1}{9}\Delta s(x) + \frac{4}{9}\Delta \bar{u}(x) + \frac{1}{9}\Delta \bar{d}(x) + \frac{1}{9}\Delta \bar{s}(x)). \tag{1.42}$$

The function $g_2(x)$ is zero in this simple model[2].

1.1.7 Fragmentation Functions

Semi-inclusive hadron measurements are very useful in separating the spin contributions by flavor. The scattered lepton is measured in coincidence with the high momentum hadrons. The scattered lepton kinematic variables determine completely the scattered quark kinematics, while the leading hadron determines the flavor of the struck quark. This kind of flavor tagging works only statistically and requires knowledge of the fragmentation functions. The HERMES results have shown that it works well when certain cuts are applied. The main cut is on the fractional energy $z = E_h/\nu$, where E_h is the energy of the hadron[2].

Due to color confinement in QCD, the outgoing quark produces a jet of hadrons. This fragmentation into hadrons can be described by a phenomenological fragmentation function, $D_f^h(z)$, which is the probability of a hadron h with energy fraction z to be produced from a quark of flavor f. The differential cross-section for producing a hadron of type h is then

$$\frac{d\sigma^h(z,x,Q^2)}{dz} = \frac{\sum_f e_f^2 q_f(x,Q^2) D_f^h(x,z)}{\sum_f e_f^2 q_f(x,Q^2)} \sigma^T(x,Q^2) \tag{1.43}$$

where $\sigma^T(x,Q^2)$ is the total DIS cross-section[2]. The fragmentation functions are normalized to the total multiplicity n_h

$$\sum_f \int_0^1 D_f^h(z)dz = n_h \tag{1.44}$$

and are constrained by momentum conservation[2]:

$$\sum_h \int_0^1 z D_f^h(z) dz = 1. \tag{1.45}$$

1.2 Sum Rules

The integrals of the quark distributions depend on the quark parton model combined with relativity effects. These integrals are used to derive the sum rules which are of great importance in DIS.

1.2.1 Bjørken Sum Rule

The Bjørken Sum rule relates the spin structure function to the axial charges g_A and g_V measured in Gamow-Teller nuclear β-decay. It is derived from pure current algebra assumptions and some QCD correction and can be expressed as:

$$\int_0^1 [g_1^p(x) - g_1^n(x)]dx = \frac{1}{6}|\frac{g_A}{g_V}| + QCD\ corrections. \tag{1.46}$$

The violation of this sum rule would cast serious doubts on the validity of the quark parton model and perturbative QCD, and experimentally the Bjørken sum rule has been confirmed[2].

1.2.2 Ellis-Jaffe Sum Rule

Using SU(3) symmetry arguments the spin fractions carried by the different quark flavors can be related to the axial coupling known from the baryon-octet decays. If we define $\Delta q_f = \int_0^1 \Delta q_f(x)$, the first moment of $g_1(x)$ can be expressed as

$$\Gamma_1^{p(n)} = \int_0^1 g_1^{p(n)}(x)dx = \frac{1}{12}(\pm a_3 + \frac{a_8}{3}) + \frac{1}{9}a_0 + QCD\ corrections \tag{1.47}$$

where

$$a_3 = g_A/g_V = F + D = \Delta u - \Delta d \tag{1.48}$$

$$a_8 = 3F - D = \Delta u + \Delta d - 2\Delta s \tag{1.49}$$

$$a_0 = \Delta\Sigma = \Delta u + \Delta d + \Delta s. \tag{1.50}$$

a_3 and a_8 are known from neutron and hyperon decay[2]. The numerical values are:

$$F = 0.459 \pm 0.008 \qquad D = 0.798 \pm 0.008. \tag{1.51}$$

$\Delta\Sigma$ is the total spin carried by the quarks. The Ellis-Jaffe sum rule is derived from the assumption that the total spin contribution of strange quarks is zero: $\Delta s = 0$. For proton and neutron the Ellis-Jaffe sum rules follow from Equation 1.47 directly:

$$\Gamma_1^p = 0.185 \qquad \Gamma_1^n = -0.024. \tag{1.52}$$

In 1987, the Ellis-Jaffe integral was measured by the EMC and was found to violate the QCD-corrected sum rule:

$$\Gamma_1^p = (0.189)_{theory} \neq (0.126 \pm 0.010 \pm 0.015)_{EMC/SLAC}. \tag{1.53}$$

The violation, which was termed the "spin crisis," was confirmed in later experiments[2].

1.2.3 The Spin Content of the Nucleon

Using the Ellis-Jaffe integrals, the spin fraction carried by each quark flavor in the nucleon can be determined. With QCD corrections to third order, the following results were obtained from the SMC and SLAC data quoted at a renormalization scale $Q^2 = 10\ GeV^2$[2]:

$$\Delta u = 0.85 \pm 0.03 \tag{1.54}$$

$$\Delta d = -0.41 \pm 0.03 \tag{1.55}$$

$$\Delta s = -0.08 \pm 0.03 \tag{1.56}$$

$$\Delta\Sigma = 0.37 \pm 0.07. \tag{1.57}$$

The total spin of the nucleon is thought to consist of four parts:

$$\frac{1}{2} = \frac{1}{2}\Delta\Sigma + \Delta L + \Delta G + \Delta L_G \tag{1.58}$$

where ΔL is the angular momentum of the quarks, ΔG is the spin carried by the gluons and ΔL_G is the angular momentum carried by the gluons.

1.3 Theoretical Motivation

The HERMES experiment is described in Chapter 2 of this thesis. Its focus is the $\Delta\Sigma$ term of Equation 1.58, which consists of the u, d and s polarization terms. The quark spin contributions are of great theoretical importance, and the Δs term remains relatively unknown. Chapter 3 of this thesis describes analysis which used the HERMES 1996 and 1997 data to measure Δs. The results of that analysis are described in Chapter 3 and are interpreted in Chapter 4. The author's conclusions are presented in Chapter 5.

Chapter 2

HERMES Experiment

HERMES, commissioned in 1995, is an experiment designed to study the spin structure of the nucleon by studying the deep inelastic scattering of polarized positrons off polarized nuclear targets. It goes beyond its predecessors at SLAC and CERN. One unique feature of HERMES is that it uses a thin gas target internal to the storage ring. It uses a longitudinally polarized positron beam, which in conjunction with the internal gas target makes HERMES a very clean experiment. HERMES is also a second generation spin structure experiment, with the capability to make semi-inclusive measurements of the final hadronic state.

2.1 HERA Accelerator Facility

The HERMES experiment uses the HERA storage ring located at DESY in Hamburg, Germany. This choice was prompted by the requirements of fast polarization build-up and sufficient beam energy to allow measurement of DIS. HERA meets those requirements with its lepton ring, which can store about 35 mA of positrons or electrons at 27.5 GeV, and build up full polarization in about 35 minutes. HERMES is located in the East Hall of the ring. There HERA's 820 GeV proton beam (used for colliding experiments) is 72 cm from the lepton beam, shielding the proton beam from the effects of the internal target[8].

The polarization of the leptons is naturally caused by a small asymmetry in the synchrotron radiation cross-section, called the Sokolov-Ternov effect. The maximum ideal polarization due to this effect is 92.38% and the polarization is transverse[9]. HERMES, however, requires longitudinal polarization to probe the spin structure of the nucleon. Thus, two spin rotators have been installed in the HERA ring, one upstream and one dowstream

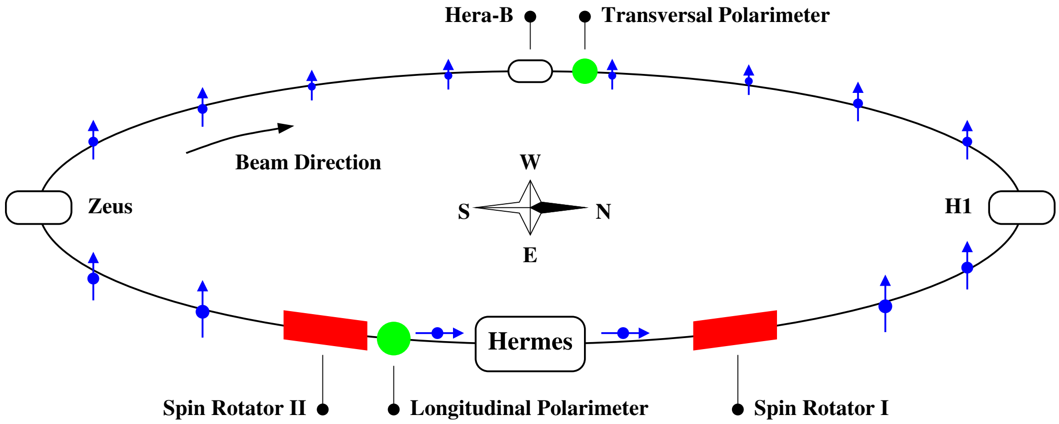

Figure 2-1: HERA storage ring with HERMES spin rotators.

from the HERMES experiment (see Figure 2-1). The maximum ideal longitudinal polarization achieved in this way is 89%. The non-uniformity of the magnetic fields, as well as quantum effects, reduce the actual polarization of the lepton beam[9]. The beam polarization is measured using a laser backscattering Compton polarimeter. There is a polarimeter located in the West Hall, which measures transverse polarization and is used with the assumption that the polarization is longitudinal to within a few degrees at HERMES. In addition, there is a longitudinal polarimeter inside the spin rotators located in the East Hall. Typical polarization is ~55%. Polarization values of up to 70% have been achieved[8].

2.2 HERMES Targets

The HERMES experiment uses internal targets in order to reduce the dilution by unpolarized nuclei, and thus reduce systematic errors. Internal targets also allow for a rapid polarization reversal, reducing time-dependent systematic errors in spin asymmetry measurements[9]. HERMES uses the novel technique of a storage cell, in which polarized gas is pumped into a T-shaped elliptical cell mounted coaxially with the HERA beam (see Figure 2-3[12]). Thus, high luminosity is achieved by increasing the density of gas in the beam path. Low gas pressure allows the use of a thin-walled cell, reducing the multiple scattering and external radiative corrections. The storage cell is cryogenically cooled, further increasing the target density. The HERMES target thickness is of order $10^{14} - 10^{15}$ polarized atoms/cm^2[8]. The gas undergoes only about a hundred wall bounces before leaving the cell, reducing the interactions with cell walls and thus the possibility of recombination.

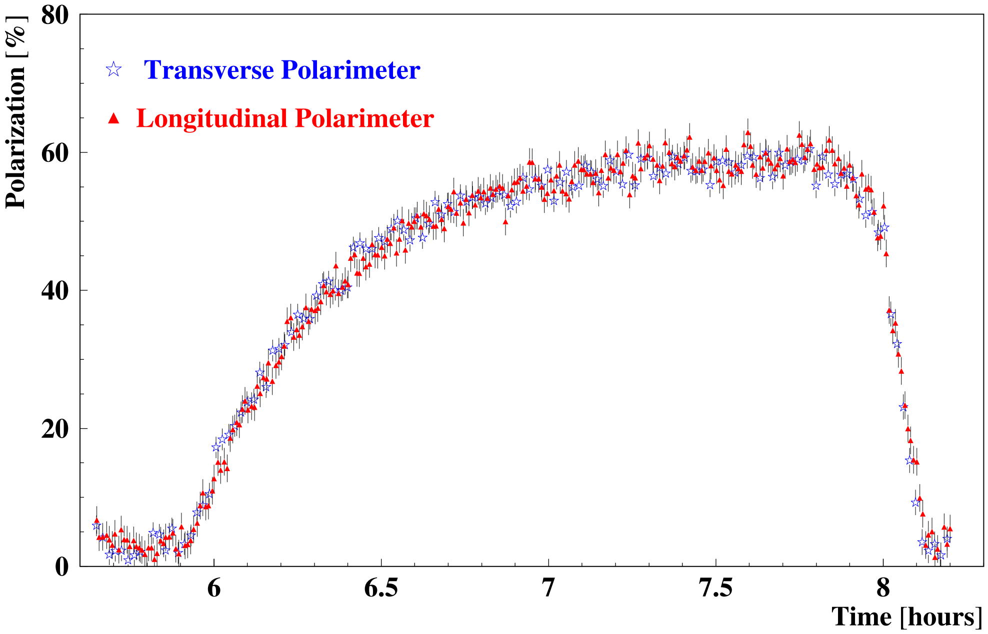

Figure 2-2: Observations of transverse and longitudinal polarization at HERMES.

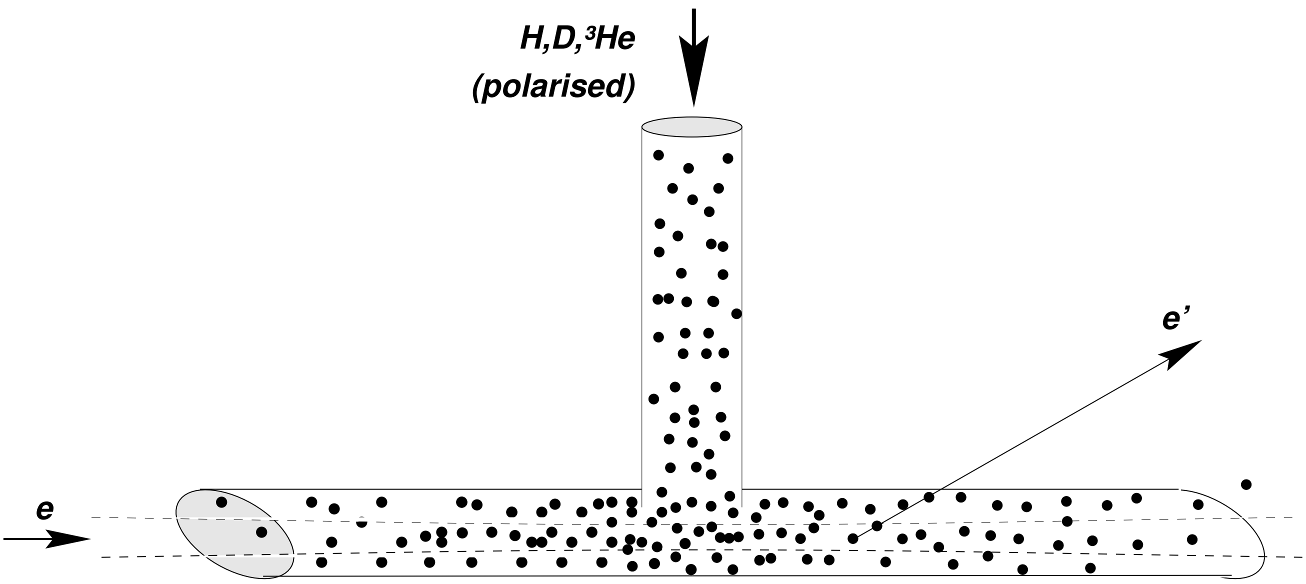

Figure 2-3: Schematic of the HERMES storage cell.

Three common targets for HERMES are hydrogen, deuterium and helium-3 targets. The sources for these targets are an optically pumped source for ^3He and an atomic beam source for hydrogen and deuterium[9]. In 1996 and 1997, the HERMES experiment used a polarized proton (hydrogen) target. The high-intensity atomic beam source produces three different pairs of hyperfine states in hydrogen gas, which passes through a sextupole magnetic field, allowing for both polarization directions. The average nuclear polarization was 0.90 for both polarization directions in 1996 and 0.92 in 1997. The average atomic fraction was 0.88 in 1996 and 0.95 in 1997, without considering testing and unpolarized runs[6]. The atomic fraction is the ratio of the atomic hydrogen flux to the total atomic flux, as measured by the HERMES target gas analyzer.

2.3 HERMES Detector

The combination of a fixed target and a high-energy beam means that the angular distribution of the scattered particles is concentrated in the forward direction. In order to study a large kinematic range, a detector must have a large angular acceptance. The HERMES detector is a forward spectrometer with a minimal vertical angle of 40 mrad, maximum vertical angle of 140 mrad and a horizontal acceptance of ± 170 mrad[9]. The detector is designed to provide a clean measurement of the scattered lepton in a wide kinematic range, as well as a good identification of the final hadronic state (see Figure 2-4[12]). The main background for the HERMES experiment comes from the synchrotron radiation, scattering of the beam halo from the collimator system and protons lost in the HERA's proton ring. The first two sources are minimized by a good beam tune. The lepton and proton bunches in the rings are out of phase and thus interference can be eliminated by a simple trigger gate. Besides the trigger, the proton background is monitored by a veto detector[9]. To monitor the luminosity, two small calorimeters are installed close to the beam downstream from the target.

2.3.1 The Tracking Detectors

The tracking detectors consist of several chambers. These chambers are divided into three regions with respect to the main spectrometer magnet: forward, back and magnet. The forward region contains two chambers, vertex chamber (VC) and forward chamber (FC),

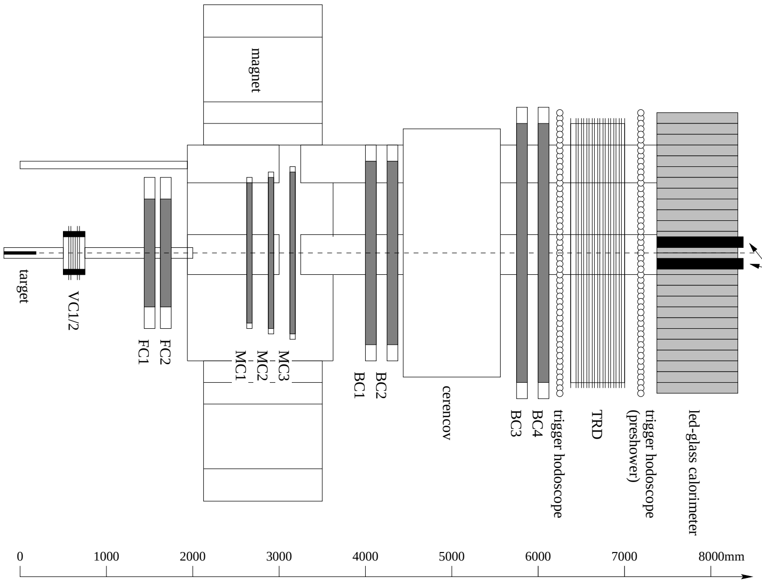

Figure 2-4: Schematic of the HERMES detector.

and is responsible for measuring the angle of the track and its scattering vertex. The vertex chamber is a micro-strip gas chamber, while the forward chamber is a drift chamber with a conventional horizontal drift configuration. The back region contains two sets of back chambers (BC) and, together with the forward region track, measures the angle of deflection of a particle in the spectrometer magnet and thus its momentum. The back chambers are of the same configuration as the forward chamber. The magnet region is responsible for matching the tracks from the forward region with those in the back region. This region contains magnet chambers (MC) and can also be used to increase the acceptance of the detector for the lower energy particles. All chambers measure the same three coordinates. This allows for a robust and rapid reconstruction of the tracks[9].

2.3.2 The Particle Identification Detectors

Both inclusive and semi-inclusive studies require clean particle identification. Most important is the distinction between leptons and hadrons, and for the semi-inclusive measurements, the identification of the hadron type. All HERMES particle identification (PID) detectors are located in the back region. The detectors that comprise the PID system are the calorimeter, the hodoscopes, the preshower detector, the Ĉerenkov and the transition radiation detector (TRD). Pions and other hadrons cause hadronic showers which travel further in the calorimeter blocks while losing energy by ionization, since the nuclear reaction length is much larger than the radiation length. A comparison of the energy deposited in the calorimeter with the energy determined by the track bending in the magnet provides a good distinction between hadrons and leptons. The Ĉerenkov detector provides a partial proton-kaon-pion separation. A newly installed ring-imaging Ĉerenkov detector (RICH) should provide full separation. The TRD detects the lesser known relative of the Ĉerenkov radiation, the transition radiation. The TRD complements the calorimeter measurements. The main function of the hodoscope (H1) is the first-level trigger, but it can also used in the time-of-flight particle identification[9].

Chapter 3

Pion Branching Fraction Analysis

The violation of the Ellis-Jaffe sum rule has stimulated interest in the polarization of the strange sea quarks in the nucleon. The combination of DIS data with hyperon decay constants in the naive quark parton model leads to the conclusion that Δs is negative. Such analysis must ignore the contribution to the nucleon spin of the gluons and assume SU(3) flavor symmetry. The HERMES RICH detector, installed in 1998, should provide a first direct measurement of the strange sea polarization, but information on this question may already be available.

This chapter describes analysis of the 1996 and 1997 HERMES data using a technique originally derived by Frankfurt *et al.*[3] and Güllenstern *et al*[4]. This pion branching fraction analysis uses the comparison of the inclusive asymmetry with the pion semi-inclusive asymmetry. In the simplest model, the difference between the two is directly proportional to the strange sea polarization.

3.1 Theory

The pion branching fraction is defined as a ratio of the semi-inclusive pion production cross-section to the inclusive lepton cross-section in DIS:

$$n^{\pm}(x,z) = \frac{\sigma^{\pi}_{\pm}}{\sigma^{e^+}_{\pm}} \tag{3.1}$$

where "+" is used for the antiparallel spin state ($\uparrow\downarrow$) and "−" for the parallel spin state ($\uparrow\uparrow$). σ^{π} refers to the total (positive and negative) pion cross-section in each spin state. In the quark parton model this relation is[3]

$$n^{\pm}(x,z) = \frac{\sum_f e_f^2 q_f^{\pm}(x) D_f^{\pi:\pm}(z)}{\sum_f e_f^2 q_f^{\pm}(x)}. \tag{3.2}$$

From Section 1.1.5, we can determine that $q_f^{\pm} = \frac{1}{2}(q_f(x) \pm \Delta q_f(x))$. $D_f^{\pi:\pm}(z)$ refers to the total pion fragmentation function for the two spin states (not to be confused with the pion charge). Making no symmetry assumptions the strange sea polarization, Δs, can be extracted from the difference of the branching fractions for each spin orientation:

$$n^{+}(x,z) - n^{-}(x,z) = \frac{1}{F_1(x)(1-A_1(x)^2)} \cdot$$

$$\left[\sum_f e_f^2 \left[\Delta q_f(x) - A_1(x) q_f(x)\right] \left[D_f^{\pi}(z) - \epsilon\right] + \right.$$

$$\left. \sum_f e_f^2 \left[q_f(x) - A_1(x)\Delta q_f(x)\right] \delta D_f^{\pi}(z) \right]. \tag{3.3}$$

In the derivation, the quark parton model result,

$$\sum_f e_f^2 [q_f(x) \pm \Delta q_f(x)] = 2F_1(x)[1 \pm A_1(x)], \tag{3.4}$$

was used. D_f^{π} is the unpolarized fragmentation function and is defined as $D_f^{\pi} = \frac{1}{2}(D_f^{\pi:+} + D_f^{\pi:-})$. δD_f^{π} is defined as $\delta D_f^{\pi} = \frac{1}{2}(D_f^{\pi:+} - D_f^{\pi:-})$. This quantity is predicted to be zero from theory. However, it may be non-zero once acceptance effects are considered. This will be further discussed in Section 3.1.3. The ϵ factor is an arbitrary factor used to facilitate later calculations. This is justified since $\sum_f e_f^2[\Delta q_f(x) - A_1(x) q_f(x)] = 0$ and thus can be multiplied by an arbitrary number without affecting the equations.

Δs can be extracted from Equation 3.3 by rearranging the terms as follows:

$$\frac{\Delta s(x) + \Delta \bar{s}(x)}{2} = A_1(x)\,\frac{s(x)+\bar{s}(x)}{2} +$$

$$\frac{1}{D_s^{\pi}(x,z) + D_{\bar{s}}^{\pi}(x,z) - 2\epsilon} \cdot \left[9F_1(x)[1 - A_1(x)^2]\left[n^{+}(x,z) - n^{-}(x,z)\right] - \right.$$

$$9 \sum_{l=u,d,\bar{u},\bar{d}} e_l^2 [\Delta q_l(x) - A_1(x) q_l(x)] \left[D_l^{\pi}(x,z) - \epsilon\right] -$$

$$9\sum_f e_f^2[q_f(x) - A_1(x)\Delta q_f(x)]\delta D_f^{\pi}(x,z)\Bigg] . \quad (3.5)$$

This is the main equation of the pion branching fraction analysis. The second term on the right hand side depends on the measured branching fractions. The third term is termed the light quark fragmentation correction (LQC) and the fourth term, the spin-dependent fragmentation correction (SDC). These terms are explained in detail in further sections. The derivation of Equation 3.5 did not take into account any QCD corrections, but these are expected to be small. When this equation is used, it is integrated over all kinematic variables, except x, which is averaged in several bins. Wherever the z or Q^2 dependence is dropped in further sections, integration over these variables is implied. The added x dependence in fragmentation functions comes from HERMES acceptance effects.

3.1.1 Determination of Branching Fractions

To calculate the branching fractions from actual data one must take into account the imperfect polarizations, depolarization factors and acceptance effects. De Schepper and Mateos[10] have derived the relations between the branching fractions and counting rates:

$$n^{\pm} = \kappa \frac{N_{\pi}^{+}\mathcal{D}^{-}LP^{-} + N_{\pi}^{-}\mathcal{D}^{+}LP^{+} \pm N_{\pi}^{+} \mp N_{\pi}^{-}L^{+}}{N_{e^+}^{+}\mathcal{D}^{-}LP^{-} + N_{e^+}^{-}\mathcal{D}^{+}LP^{+} \pm N_{e^+}^{+}L^{-} \mp N_{e^+}^{-}L^{+}} \quad (3.6)$$

where $N_{\pi}^{\pm}$ are the total pion counts in each spin state and $N_{e^+}^{\pm}$ are the total DIS counts in each spin state. $L^{\pm}$ represents the luminosity factors, while $LP^{\pm}$ is the luminosity multiplied by the beam and target polarizations. $\mathcal{D}^{\pm}$ is the depolarization factor defined in Section 1.1.4 for each spin state. κ is a factor that corrects for the acceptance differences between the inclusive and semi-inclusive processes so that the cross-section is calculated in 4π. This factor is estimated through Monte Carlo simulations and is approximately 2 for the HERMES data. Different methods used to verify this factor are discussed in Section 3.5.4.

3.2 The Simplest Model

SU(3) symmetry arguments imply that charge conjugation and isospin are good fragmentation symmetries. This means that

$$D_u^\pi = D_d^\pi = D_{\bar{u}}^\pi = D_{\bar{d}}^\pi \equiv D^\pi. \tag{3.7}$$

If ϵ is chosen to be equal to D^π then the LQC term of Equation 3.5 vanishes.

Theoretical fragmentation models imply no fragmentation dependence on the spin state. Thus, it is possible to assume that $D^{\pi:+} = D^{\pi:-}$. If this is true, then the fourth term of Equation 3.5, SDC, vanishes as well. If $s(x)$ and $\bar{s}(x)$ are also assumed to have identical properties, Equation 3.5 becomes

$$\Delta s(x) = \frac{1}{D_s^\pi(x) - D^\pi(x)} 9F_1(x)[1 - A_1(x)^2][n^+(x) - n^-(x)] + A_1(x)s(x). \tag{3.8}$$

A similar relation can be derived for the sum of branching ratios, leaving two equations with two unknowns, Δs and D_s^π. This is the formalism of Frankfurt *et al*[3]. The dependence on relatively poorly known D_s^π can thus be eliminated.

In this work, however, we keep the explicit D_s^π dependence in order to test the validity of the symmetry assumptions. The values for D_s^π come from the Monte Carlo fits to HERMES pion and hadron yields. With the future HERMES RICH measurements, the systematic uncertainty in D_s^π may be significantly reduced.

3.3 Rigorous Treatment

The implicit extraction of D_s^π from the very limited polarized statistics by Frankfurt[3] may make the Δs measurement statistically impossible. In addition, the analysis of the LQC and SDC terms of Equation 3.5 by the author suggests that both of these terms may be significant in the Δs measurement.

3.3.1 Spin Dependent Fragmentation Correction

In theory, factorization models imply no differnce between $D^{\pi:+}$ and $D^{\pi:-}$ (from this point on, D^π refers to the average of the four light quark fragmentation functions). However, when measured pion yields are considered, acceptance effects must be taken into account. These acceptance effects may produce spin dependence in the effective fragmentation function. In the analysis of the parton distribution as functions of x, the effective fragmentation function for a quark of flavor f to pions in one x bin is[11]

$$D^{\pi:\pm}_{eff,xbin} = \frac{\int_{x_{low}}^{x_{high}} dx \int_{1.0}^{\infty} dQ^2 q_f^{\pm}(x,Q^2) \int_{0.2}^{1.0} dz D^{\pi}(z)\mathcal{A}(x,Q^2,z)}{\int_{x_{low}}^{x_{high}} dx \int_{1.0} dQ^2 q_f^{\pm}(x,Q^2)} \tag{3.9}$$

where $\mathcal{A}(x,Q^2,z)$ is the acceptance of the detector. D^{π}_{eff} is the function used for the fragmentation function D^{π}_{f} in this analysis. The parton distributions $q_f^{\pm}(x,Q^2)$ are spin-dependent, while the acceptance strongly depends on x and Q^2. Integrating over all variables but x, hadron acceptance of HERMES is inversely proportional to x. Thus, if the quark distribution in one spin state has higher average x than in the other spin state, then that spin state will have a smaller acceptance, and thus a smaller effective fragmentation function. For example,

$$(\langle x\rangle^{-} > \langle x\rangle^{+}) \rightarrow (\mathcal{A}^{-} < \mathcal{A}^{+}) \rightarrow (D^{\pi:-}_{eff} < D^{\pi:-}_{eff}). \tag{3.10}$$

Thus, there may be spin dependence in the fragmentation. In the analysis of u and d quark polarizations this dependence was found to be negligible. However, strange sea polarization is significantly smaller than light sea plarization and so the spin dependent fragmentation effects cannot be ignored. These effect are represented by the SDC term of Equation 3.5.

3.3.2 Light Quark Fragmentation Correction

The assumption of charge conjugation in fragmentation may be broken at a level that affects the Δs measurement. There are two separate possible causes for this effect. First, the true fragmentaion function may not be symmetric under charge conjugation. In fact, the LUND Monte Carlo predicts that some symmetry breaking occurs at HERMES energies. Secondly, acceptance effects, similar to those described in Section 3.3.1 may contribute to the asymmetry in fragmentation. In a given x bin, at low x parton distributions are larger for sea quarks than for valence quarks. As x increases the sea contribution drops off exponentially, while the valence contribution remains relatively the same. Therefore, in most x bins $\langle x\rangle_{sea} < \langle x\rangle_{valence}$. Using arguments of Section 3.3.1, the effective fragmentation is thus higher for sea quarks as compared to valence quarks. Since all anti-quarks are found

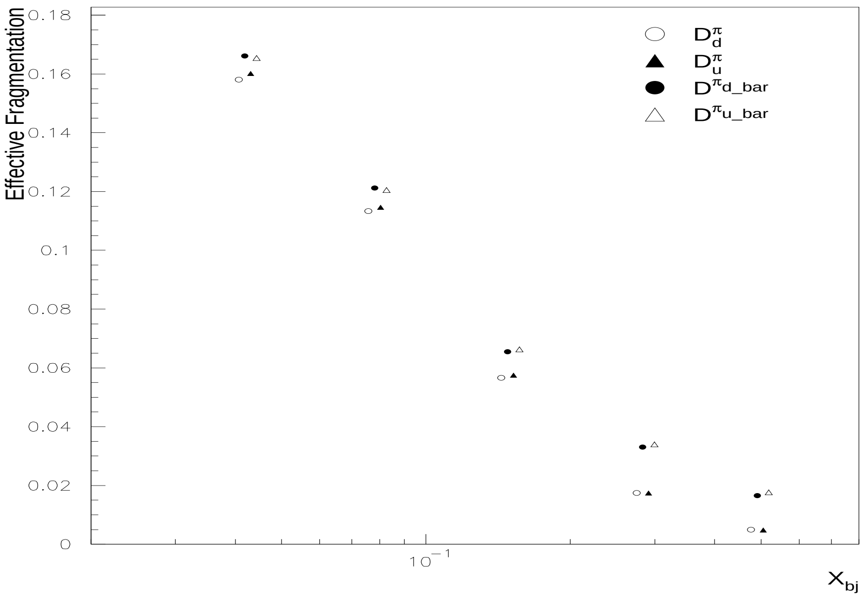

Figure 3-1: A comparison of the pion fragmentation functions for the 4 light quark flavors derived from the LUND string model fitted to HERMES data.

in the sea this results in the breaking of the charge conjugation symmetry:

$$D^{\pi}_{q} \neq D^{\pi}_{\bar{q}}. \tag{3.11}$$

Figure 3-1 shows the fragmentation function D^{π} versus x for the light quarks as determined by the LUND string fragmentation model fitted to HERMES hadron data. The charge conjugation symmetry is broken at the level of 5%. This effect does not allow the cancellation of the light quark polarizations in the calculation of branching fractions. This introduces a background in the Δs, which is enhanced by the charge factors of the light quarks and their large polarizations (relative to the expected strange quark polarization). The LQC term of Equation 3.5 reflects this symmetry breaking effect and isolates the background noise. However, in this work the LQC term is estimated from HERMES Monte Carlo studies, and, since fragmentation symmetry breaking has never been measured, is a source of a systematic uncertaity. This is further discussed in Section 3.5.3.

3.3.3 The ϵ factor

If the charge conjugation symmetry in fragmentation is broken, there is no ϵ factor that can completely cancel the LQC term of Equation 3.5. The choice of new ϵ has certain effects on the calculations. This term was introduced as an arbitrary factor. However, there are some limits that have to be respected.

All terms of Equation 3.5, except the LQC term, are of order $\frac{1}{\epsilon}$. If we take the limit $\epsilon \to \infty$, all terms of the Equation 3.5 except the LQC term vanish and the equation becomes

$$\frac{\Delta s(x) + \Delta \bar{s}(x)}{2} = A_1(x)\frac{s(x) + \bar{s}(x)}{2} - \frac{9}{2}\sum_{l=u,d,\bar{u},\bar{d}} e_l^2[\Delta q_l(x) - A_1(x) q_l(x)] \tag{3.12}$$

which is an identity in the quark parton model independent of the measured data (all data have been divided by $\epsilon = \infty$). Since the LQC term is calculated by Monte Carlo, if ϵ is large, the measured value of Δs will be influenced by the Monte Carlo. In order to make the measurement, an iterative procedure is necessary which will put back the result of the previous step until the input and output converge. Another way to accomplish this is to choose an ϵ that initially minimizes the LQC term of Equation 3.5. The best choice of ϵ is the average of all light quark pion fragmentation functions.

It is important to note that if $2\epsilon = D_s^\pi + D_{\bar{s}}^\pi$, Equation 3.5 will diverge. Physically this means that the strange quark fragmentation to pions is nearly equal to the light quark fragmentation to pions. In such a case the difference between the pion asymmetry and inclusive asymmetry is not sensitive to Δs. Section 3.3.4 shows that such a divergence is predicted by HERMES Monte Carlo at high x.

3.3.4 The D_s^π Dependence

Figure 3-2 shows the average effective fragmentation of strange quarks compared to the average effective fragmentation of light quarks (the choice of ϵ in this work). The values were obtained from the PEPSI simulation using the string fragmentation parameters fitted to HERMES hadron data. Theoretically it is expected that $D_s^\pi < D^\pi$. As seen from Figure 3-2, this relation holds for low x. However, at high x, the Monte Carlo predicts that $D_s^\pi > D^\pi$. The measurement of Δs may diverge around $x = 0.2$ as discussed in Section 3.3.3. This result is reasonable (though unexpected) when the accepted yields are integrated over x and Q^2, since the tagged strange quark events occur at lower x and higher Q^2 in

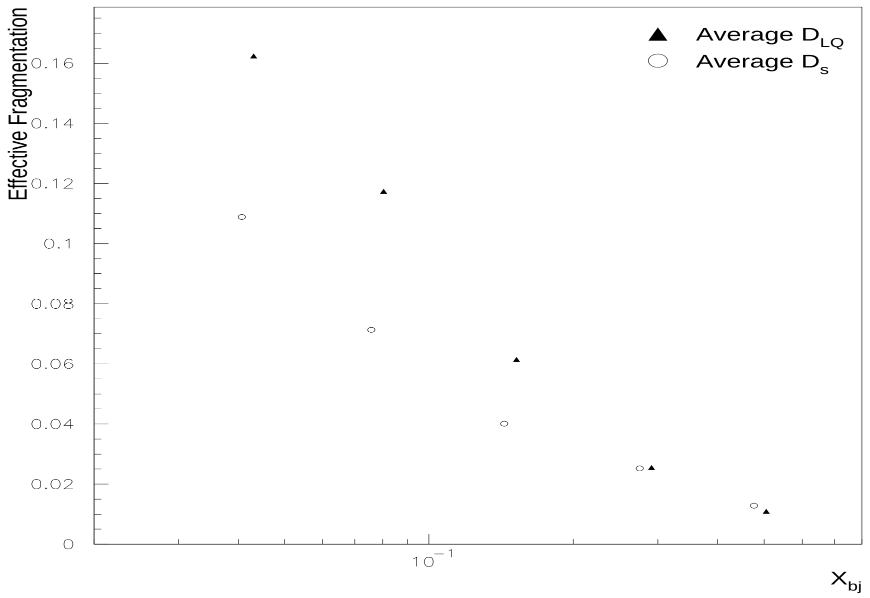

Figure 3-2: The average light quark fragmentation to pions compared to the average strange quark fragmentation to pions.

any x bin according to the PEPSI simulation. The strong kinematic dependence of the HERMES acceptance may favor these strange quark events.

In Equation 3.5, $D_s^\pi - D^\pi$ appears as an analyzing power, and as long as it is assumed that $0 < D_s^\pi < D^\pi$, then the sign and the relative statistical uncertainty in the Δs measurement are independent of uncertainty in the strange quark fragmentation.

3.3.5 Explicit Formalism

The formalism described above is exact, but it may be tedious to the reader. There is a way to explicitly show the dependence of the branching fractions difference on the measured asymmetries:

$$n^+(x) - n^-(x) \sim 2D^\pi [A_1^\pi(x) - A_1^{e^+}(x)]. \quad (3.13)$$

This expression provides a more intuitive model for the source of the strange sea polarization signal. Figures 3-3 and 3-4 show the measured inclusive ($A_1^{e^+}$), semi-inclusive all-hadron (A_1^h) and semi-inclusive pion (A_1^π) asymmetries for 1996 and 1997 proton data. From these figures we conclude that A_1^π is smaller than A_1^h and $A_1^{e^+}$ over most of the x range.

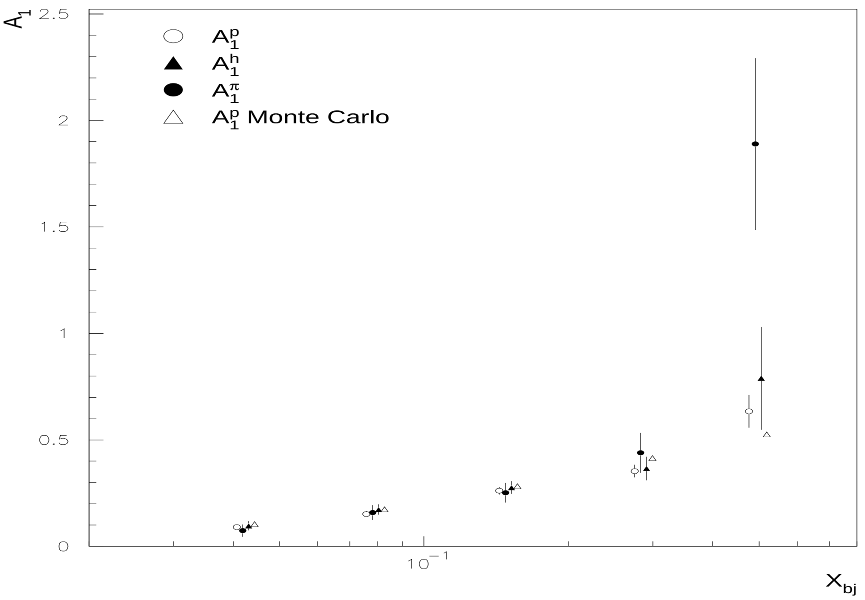

Figure 3-3: A comparison of 1996 semi-inclusive all-hadron, pion and inclusive assymetries.

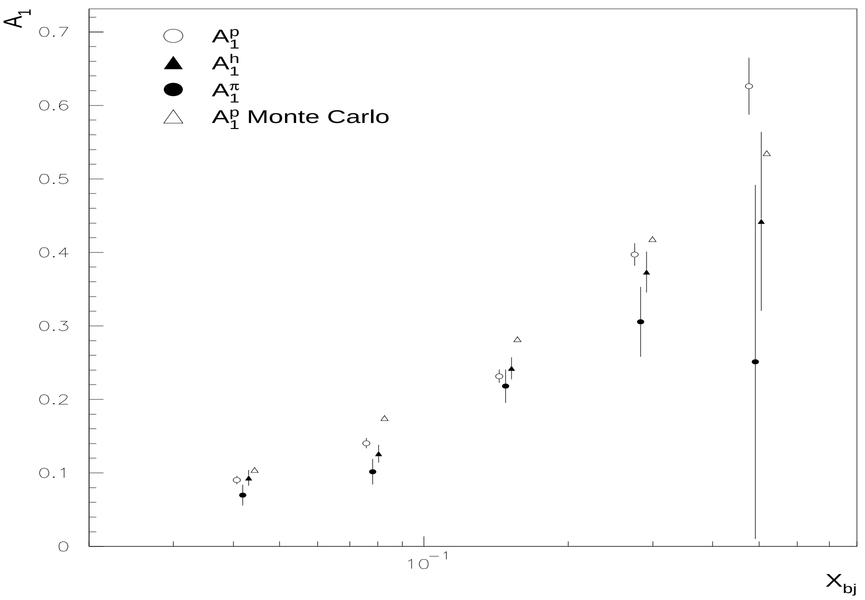

Figure 3-4: A comparison of 1997 semi-inclusive all-hadron, pion and inclusive assymetries.

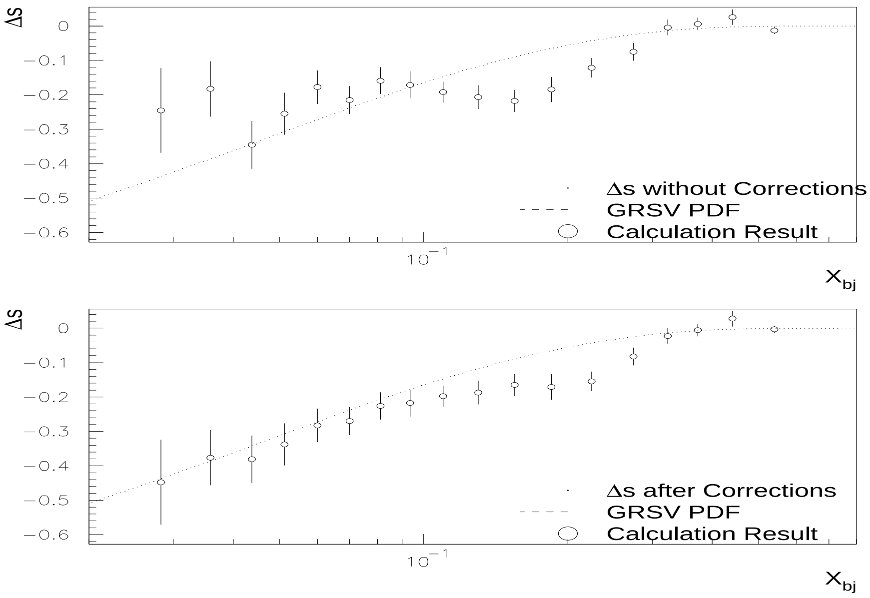

Figure 3-5: The inversion of the Monte Carlo in the branching fraction analysis. The dotted line represents the input Δs.

3.4 Monte Carlo Simulation and Testing

The first step is to test the procedure described in the previous sections. This can be done by applying the analysis to the Monte Carlo simulation where the input strange sea polarization is known. The output can then be compared with the input to verify the validity of the measurement.

For this test the PEPSI Monte Carlo was run with the string fragmentation parameters fitted to HERMES data. GRV parton distribution functions were used. The data cuts applied to the Monte Carlo were the same as those applied to the data (see Section 3.5.1). Figure 3-5 shows the extracted Δs compared to the GRSV predicted Δs at HERMES Q^2. The top plot shows the uncorrected Δs, that is the LQC and SDC terms of Equation 3.5 have been set to zero (in other words, Equation 3.8 was used). The bottom plot shows the full corrected measurement. It is seen from these graphs that the corrections are necessary to achieve close agreement between the input and the extraction. It is also notable that around $x = 0.2$ the agreement is lost because PEPSI predicts that $D_s^\pi \sim D^\pi$ in that region as discussed in Section 3.3.3. The origin and calculation of the statistical errors will be addressed in Section 3.5.3.

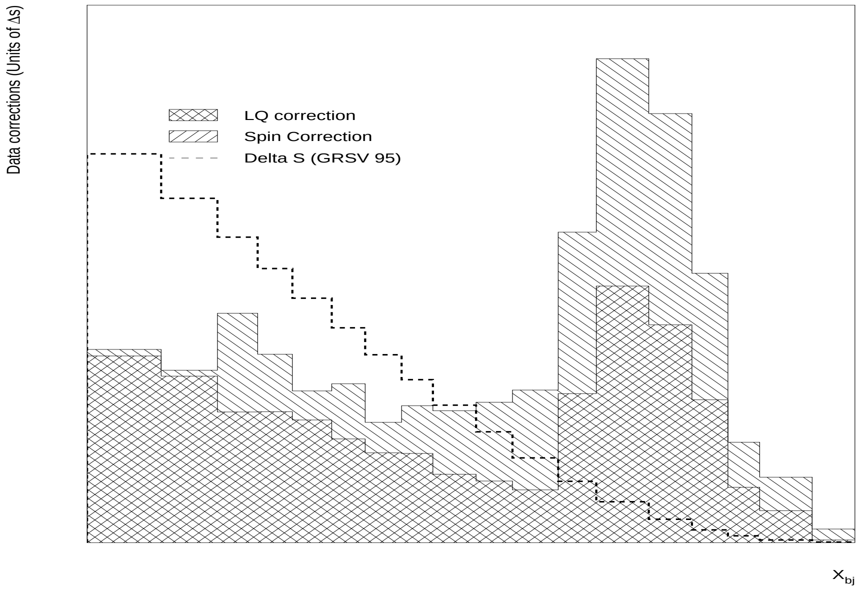

Figure 3-6: Corrections in the branching fractions analysis from PEPSI in 18 x bins used for Monte Carlo studies.

The size of the corrections can be directly seen in Figure 3-6, where the cross-hatched area represents the light quark fragmentation correction, and the spin-dependent fragmentation correction is added on top as a single-hatched area. The predicted GRSV parameterization is shown as a dotted line for comparison.

Throughout the further analysis, this work uses five x bins. Figure 3-7 shows the same corrections to Figure 3-5 using these five bins. As noted in Sections 3.3.1 and 3.3.2, some of the corrections arise in the differences in $\langle x \rangle$ among the parton distributions in each x bin. Thus, it is expected that the corrections would increase in the wider x bins. This behavior is seen in the difference between Figures 3-6 and 3-7.

In the Monte Carlo testing, the LQC and SDC terms were nearly equal to the expected Δs signal. Since neither correction is well understood, this background may have limited the feasibility of the measurement. However, the signal found in the actual data is much larger then the predicted value and the correction terms.

3.5 1996 and 1997 Data Analysis

3.5.1 Data Content and Quality

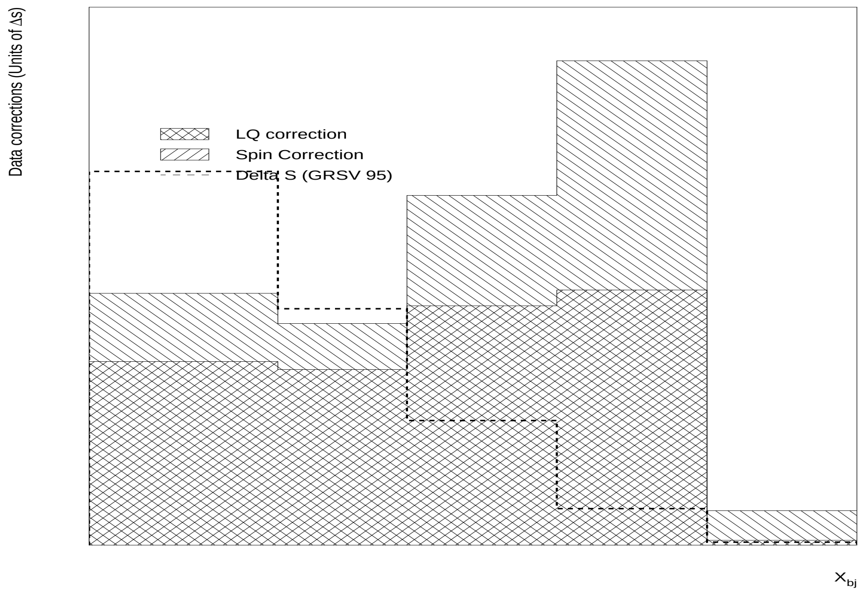

Figure 3-7: Corrections in the branching fractions analysis from PEPSI in 5 x bins used for Monte Carlo studies.

Table 3.1: HERMES data content and quality for 1996 and 1997.

	1996 Data	1997 Data
Runs	3319	7720
Bursts	133220	389851
Pion Counts	60091	158313
DIS Counts	553303	1686591
Total Hadron Counts	114228	368861
Average Luminosity	107.33	100.04
Average Polarization ($P_B \cdot P_T$)	.414	.465

The data selection consisted of several cuts. To identify DIS positron candidates the standard cuts were applied[11]:

- PID3+PID5>2,
- $Q^2 > 1$,
- $W^2 > 4$,
- $y < 0.85$,
- -18 cm$< z_{vertex} < 18$ cm,
- Transverse Vertex Position< 0.75 cm,

- 0.04 rad$< \theta_y <$0.14 rad,
- -0.17 rad$< \theta_x <$0.17 rad,
- track is not a magnet track.

Semi-inclusive hadron events are a subset of the above data set with the following cuts[11]:

- $W^2 > 10$,

and a coincident hadron has

- PID3+PID5$<$ 0,
- -18 cm$< z_{vertex} <$ 18 cm,
- 0.04 rad$< \theta_y <$0.14 rad,
- -0.17 rad$< \theta_x <$0.17 rad,
- $z_{hadron} > 0.2$,
- $x_{Feynman} > 0.1$,
- track is not a magnet track.

To identify charged pion events further cuts are applied[11]:

- $PulsCher_{hadron} > 0.25$,
- 4.9 GeV/c$< p_{hadron} <$13.3 GeV/c.

Also, no pion candidate can be closer than 52 cm in x-distance to any other Ĉerenkov track at the z position of the Ĉerenkov detector[11].

The above cuts are applied to the data throughout this analysis and are modeled in the Monte Carlo simulations.

3.5.2 Results

Figure 3-8 shows the measurement of the strange sea polarization in the combined 1996 and 1997 HERMES data using the pion branching fraction analysis. The plot shows the five x bins used throughout this analysis. The values in this plot are the full corrected values,

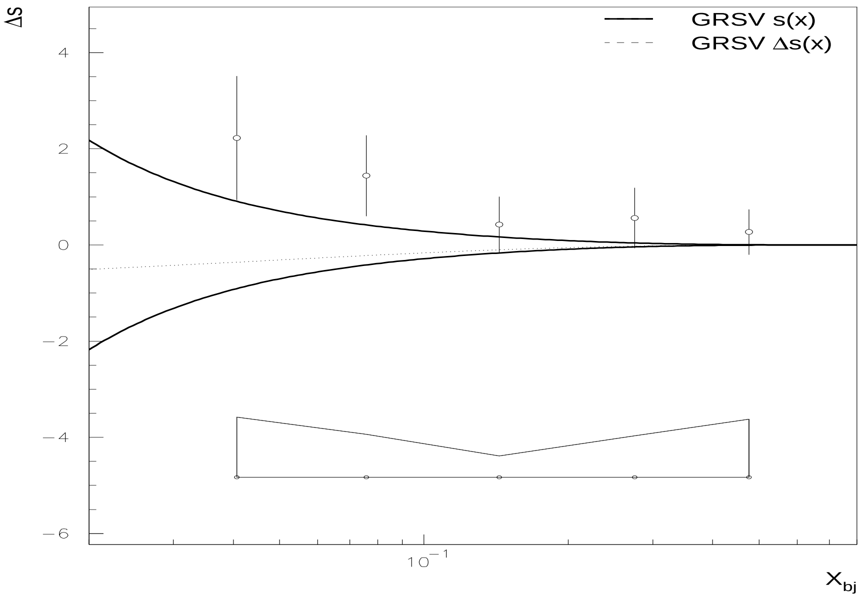

Figure 3-8: $\frac{1}{2}(\Delta s+\Delta\bar{s})$ extracted from 1996 and 1997 data using branching fraction analysis.

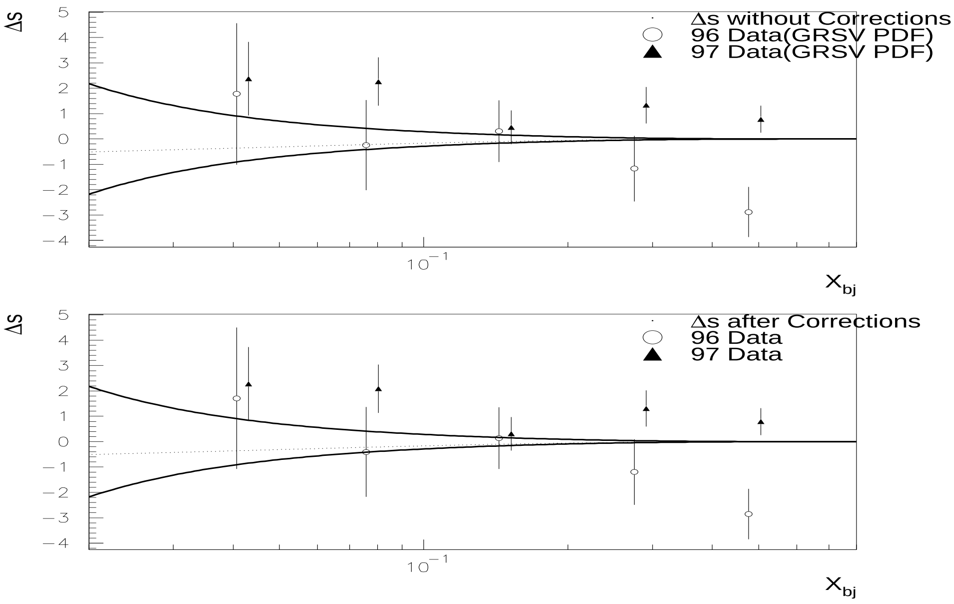

Figure 3-9: $\frac{1}{2}(\Delta s+\Delta\bar{s})$ extracted from 1996 and 1997 data using branching fraction analysis.

however, the LQC and SDC terms are extremely small compared to the Δs signal. Figure 3-9 shows the result broken down by the two years. The top plot shows the uncorrected values, while the bottom one contains the full corrected version. It can be seen that the corrections are negligible in these plots.

As can be seen from these plots, both 1996 and 1997 data sets suggest a strong positive polarization in the strange sea quarks at low x. At high x, the region of the largest statistical and systematic uncertainty, the data from the two years disagree. Because of the large uncertainty in the measurement at high x, and the very small unpolarized sea quark distributions in this region, in this work the sea polarization is set to zero above $x = 0.3$.

Integrating the first three x bins of the measurement provides the measured region contribution of strange quarks to nucleon spin. The integrals evaluated at $Q^2 = 2.5$ GeV^2 are

$$(\Delta s + \Delta\bar{s})_{1996} = 0.202 \pm 0.399 \pm 0.136 \quad (3.14)$$

$$(\Delta s + \Delta\bar{s})_{1997} = 0.551 \pm 0.212 \pm 0.321 \quad (3.15)$$

$$(\Delta s + \Delta\bar{s})_{1996+1997} = 0.402 \pm 0.187 \pm 0.359. \quad (3.16)$$

The origins and calculations of uncertainties are explained in Section 3.5.3.

3.5.3 Uncertainty Analysis

The results quoted in Section 3.5.2 were subjected to rigorous studies and uncertainty analysis. In this work the counts and other data values used in the analysis are randomly fluctuated according to a Gaussian distribution with a width equal to the measured input uncertainties. The large number of counts makes a Gaussian function a good approximation to the Poisson distribution of counting rates. These fluctuations are then propagated through Equation 3.5 producing a distribution of the result. This method was compared to the exact analytical error analysis of Equation 3.8 (the simplest case) and found to be within 10% of the correct analytical uncertainty.

Note on Statistical Uncertainty

According to the explicit formalism of Section 3.3.5 the branching fraction difference is proportional to the difference between the inclusive and semi-inclusive pion asymmetries.

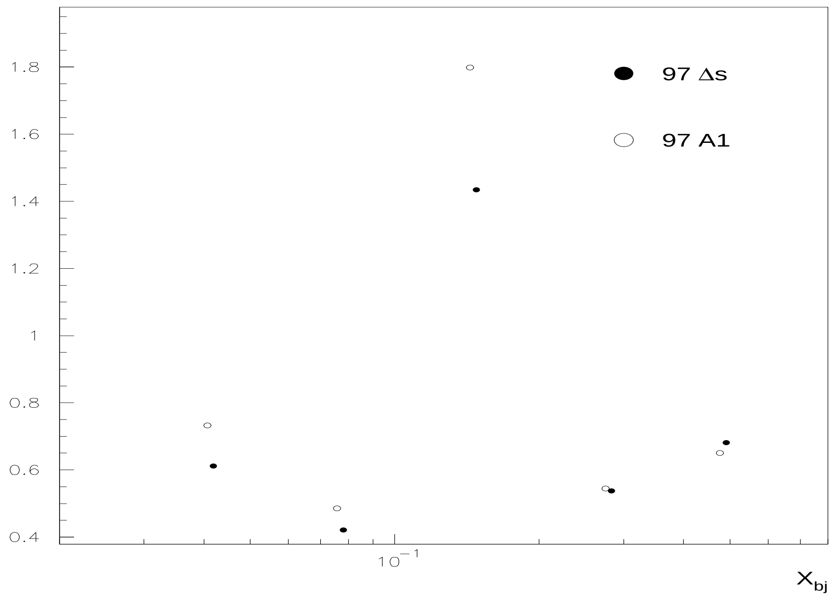

Figure 3-10: Fractional statistical uncertainty $\frac{\delta \Delta s}{\Delta s}$ compared with $\frac{\delta(A_1^\pi - A_1^{e^+})}{(A_1^\pi - A_1^{e^+})}$ for 1997 data.

It is then possible to express the fractional uncertainty in Δs in terms of the fractional uncertainty of the asymmetries:

$$\frac{\delta \Delta s}{\Delta s} = \frac{\delta(A_1^\pi - A_1^{e^+})}{(A_1^\pi - A_1^{e^+})} \tag{3.17}$$

This relation is checked for 1997 data in Figure 3-10. There is a good agreement between the fractional Δs uncertainty and the fractional asymmetry difference uncertainty. It is notable that exact agreement is not expected in Figure 3-10 since inclusive/semi-inclusive correlations were not included in the calculation of $\delta(A_1^\pi - A_1^{e^+})$.

Systematic Uncertainties

There are three main sources of systematic uncertainty. The first is the HERMES data uncertainty which is part of all data. It is manifested in the systematic uncertainty in the beam and target polarizations. In 1996, this relative uncertainty was 7% and in 1997 it was 5%. The second source of systematic uncertainty is the "theoretical uncertainty." The different parameterizations of the parton distribution functions and the different fragmentaion models affect the analysis. The relative PDF systematic uncertainty was taken from the difference of the CTEQ and GRV parameterizations and is 3.29%. The relative fragmentation model uncertainty comes from the difference in string fragmentation fits to HERMES data and is 0.87%. The final source of the systematic uncertainty is the light quark and spin-dependent fragmentation corrections themselves. The relative size of the corrections can be seen in Figure 3-7 and both have been fully included into the uncertainty.

3.5.4 Other Studies of the Results

Two significant studies were performed to understand the results of Section 3.5.2.

Acceptance Corrections

In Section 3.1.1 it was mentioned that the calculation of the branching fractions requires a large acceptance correction. Three possible ways of applying this correction were studied.

The first way is to directly calculate the average κ of Equation 3.6 in one x bin using the Monte Carlo simulation. This results in the true pion branching fractions in 4π. The second way is to ignore the κ factor in the branching fraction calculation and instead calculate the pion branching inside the HERMES acceptance. In this case, the effective fragmentation functions are used in Equation 3.5. This method should be nearly identical to the first one. The third way is to carefully treat the x and Q^2 dependence of the HERMES acceptance by correcting pion yields in the finest (x, Q^2) bins. Then the yields are combined to calculate the pion branching fractions.

For most of the analysis in this work, the second method was used. All three approaches have been studied and the results are compared in Figure 3-11. For the third method, 18 x bins and 3 y bins were used. There are small deviations between the three methods, but all invariably support the positive Δs result.

Semi-Inclusive Data Only Study

The results of Section 3.5.2 compare inclusive and semi-inclusive pion data. If there exists an unknown hadron detection bias in the HERMES acceptance then it may influence the comparison and the result. In order to test for this effect, semi-inclusive all-hadron and semi-inclusive pion data were compared, thus eliminating any bias that may be present. In this "semi-inclusive only" comparison the hadron fragmentation function were assumed to

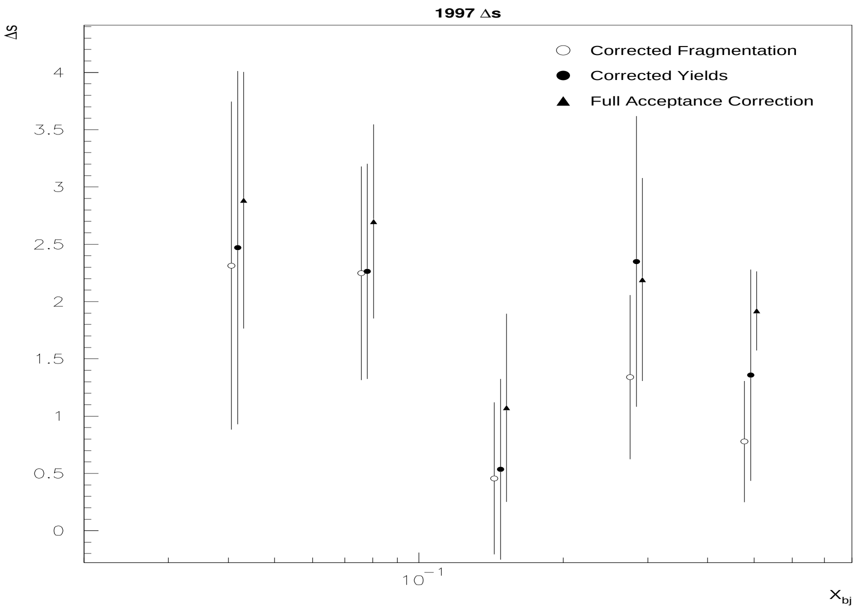

Figure 3-11: Comparison of three acceptance correction methods in the extraction of the strange sea polarization.

be independent of the struck quark:

$$D^h = D_u^h = D_d^h = D_{\bar{u}}^h = D_{\bar{d}}^h = D_s^h = D_{\bar{s}}^h \tag{3.18}$$

which is approximately true in the LUND Monte Carlo model. The new branching fractions are defined similar to Equation 3.1:

$$n_h^{\pm}(x,z) = \frac{\sigma_{\pm}^{\pi}}{\sigma_{\pm}^{h}} \sim \frac{\sigma_{\pm}^{\pi}}{\sigma_{\pm}^{e^+} D^h} \sim \frac{1}{D^h} n^{\pm}(x,z) \tag{3.19}$$

The results of this approach are shown in Figure 3-12. The positive strange polarization signal remains even when only semi-inclusive data in used.

3.5.5 Purity Analysis Results

There is another approach which uses the measured assymetries that can be used to extract the strange sea polarization. This "purity analysis" is a matrix-based method and is a standard analysis technique used by HERMES. It has succesfully been used to extract the light quark polarizations with high precision. Tipton has used the same approach to extract

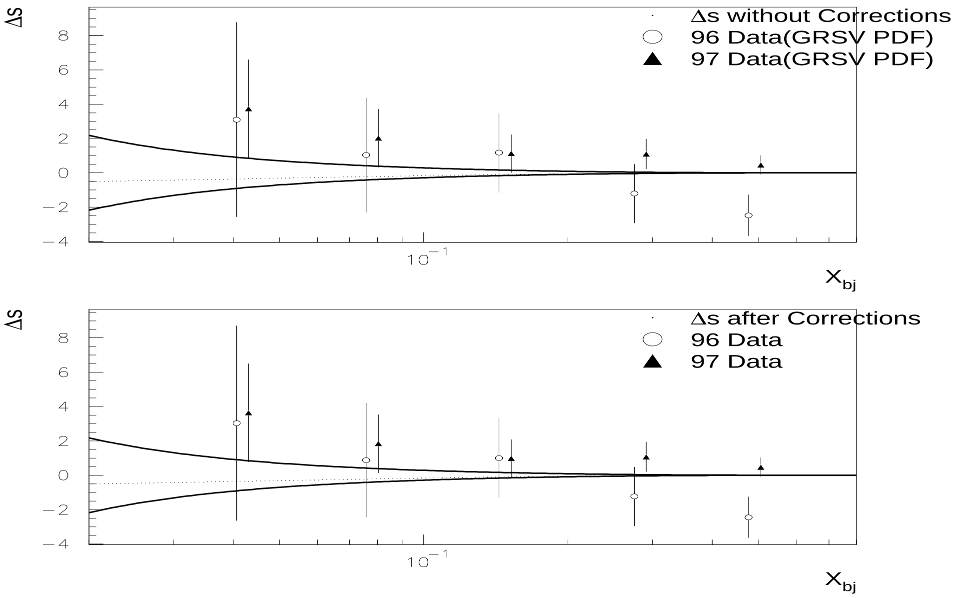

Figure 3-12: $\frac{1}{2}\Delta s+\Delta\bar{s}$ extracted from 1996 and 1997 data using branching fractions analysis using only HERMES semi-inclusive data.

the strange quark polarization[11]. Figure 3-13[11] shows the comparison between Tipton's results and the results of this work. Both show a strong positive signal for Δs at low x. Although the same data was used in both analyses, purity analysis uses a more global fit of all quark distributions, while the branching fractions method cleanly expresses the dependence of the results on fragmentation properties. The two techniques thus complement each other and their results are consistent.

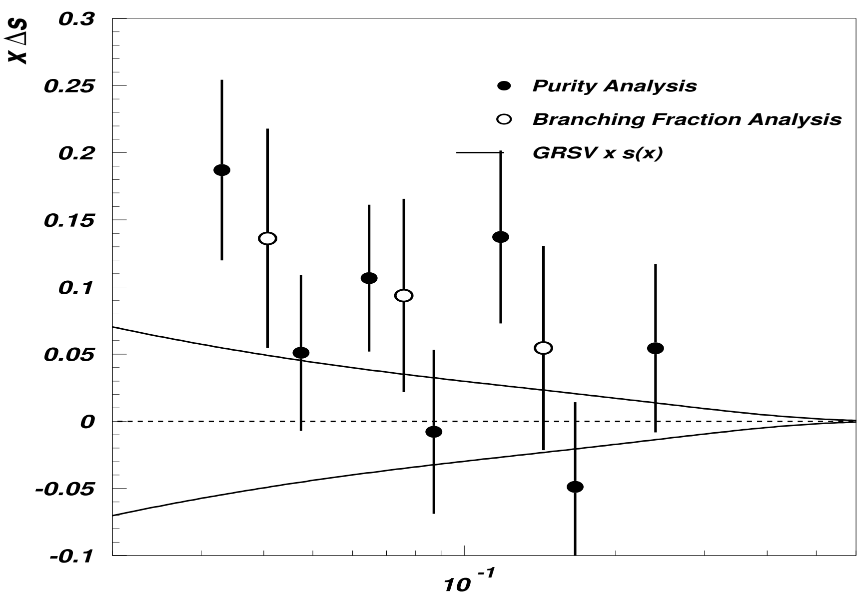

Figure 3-13: Comparison of $\frac{1}{2}x(\Delta s + \Delta\bar{s})$ from the purity and branching fractions analyses using 1996 and 1997 data.

Chapter 4

Interpretation of the Results

4.1 The Main Result

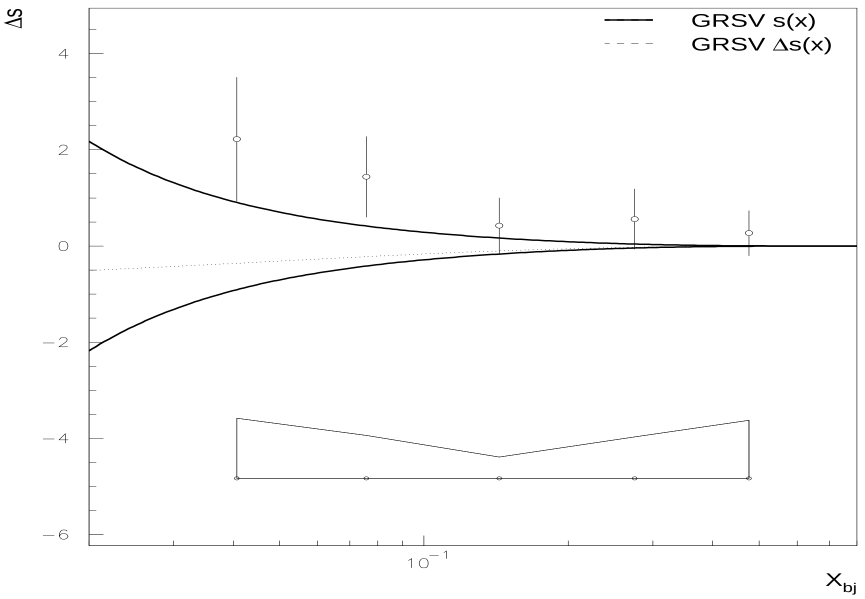

Figure 4-1: Strange sea polarization extracted from HERMES 1996 and 1997 data (same as Figure 3-8).

Figure 4-1 shows the main result of this work. It depicts a maximally positively polarized strange sea in the nucleon. Certain assumptions are made in order to come to this conclusion. The validity of the quark parton model is assumed. Factorization is assumed; that is fragmentation functions and parton distributions separate as in Equation 3.2. The LUND string fragmentation model, as fitted to HERMES hadron and pion yields, is assumed to be valid, as are the GRV unpolarized parton distribution functions. No fragmentation symmetry assumptions are made and it is assumed that the HERMES acceptance description is correct.

If some of the above assumptions are incorrect, there are several possible explanations for the results, besides the simple interpretation. Four possible interpretations are discussed in this chapter, including the naive polarized strange sea result.

4.2 Incorrect Fragmentation Models

The symmetry breaking in fragmentation contributes a sizable correction to the pion branching fraction analysis. The correction, although of the same size as the expected PEPSI Δs signal, is much smaller than the measured signal. However, if the fragmentation symmetry breaking is greatly underestimated in the Monte Carlo, the entire measured signal may originate in the light quark polarization background. The light quark correction has contributions from the binning and acceptance effects, as described in Section 3.3.2, but these contributions are assumed to be well understood in the Monte Carlo. True symmetry breaking in the 4π is also predicted by the Monte Carlo but has not been measured experimentally.

As shown in Figure 3-1, the charge conjugation symmetry breaking in HERMES fragmentation is predicted by the LUND Monte Carlo at the level of 5%:

$$D_{\bar{u}}^{\pi} \sim 1.05 D_{u}^{\pi}. \tag{4.1}$$

Using Equation 3.5 it is possible to determine the size of this symmetry breaking that will account for the measured asymmetry differences. To make the average "Δs" at low x in Figure 3-8 zero after the corrections are applied, the symmetry breaking would have to be about 25%:

$$D_{\bar{u}}^{\pi} \sim 1.25 D_{u}^{\pi}. \tag{4.2}$$

Pion yield measurements on multiple targets may be sensitive to the symmetry breaking effects in fragmentation. In the quark parton model the pion yields on an unpolarized target with Z protons and N neutrons can be expressed as:

$$
\begin{aligned}
\frac{\sigma^{\pi^+}}{\sigma^{e^+}} = \frac{1}{\kappa}[4(Zu+Nd)D_1 \quad &+ \\
(Zd+Nu)\mathbf{I}D_2 \quad &+ \quad 4(Z\bar{u}+N\bar{d})\mathbf{C}D_1 + (Z\bar{d}+N\bar{u})\mathbf{CI}D_2 + (s+\bar{s})D_2] \quad (4.3) \\
\frac{\sigma^{\pi^-}}{\sigma^{e^+}} = \frac{1}{\kappa}[4(Zu+Nd)D_2 \quad &+ \\
(Zd+Nu)\mathbf{I}D_1 \quad &+ \quad 4(Z\bar{u}+N\bar{d})\mathbf{C}D_2 + (Z\bar{d}+N\bar{u})\mathbf{CI}D_1 + (s+\bar{s})D_2] \quad (4.4)
\end{aligned}
$$

where $\kappa = (4Z+N)(u+\bar{u}) + (4N+Z)(d+\bar{d}) + (N+Z)(s+\bar{s})$[11]. Here, the notation of Geiger[7] is used and D_1 is the favored fragmetation function, while D_2 is the unfavored one. It is also assumed that the strange fragmentation function is equal to D_2. The parton distributions are a function of x and the other two variables reppresent symmetry breaking and are defined as follows:

$$D_u^{\pi^+}(z) = D_1(z) \quad (4.5)$$

$$D_d^{\pi^-}(z) = D_1(z)\mathbf{I}(z) \quad (4.6)$$

$$D_{\bar{u}}^{\pi^-}(z) = D_1(z)\mathbf{C}(z) \quad (4.7)$$

$$D_{\bar{d}}^{\pi^+}(z) = D_1(z)\mathbf{C}(z)\mathbf{I}(z) \quad (4.8)$$

and similarly for the unfavored functions.

Hence, Equations 4.3 and 4.4 contain four unknowns, $D_1, D_2, \mathbf{C}$, and $\mathbf{I}$. There are only two equations for any given unpolarized target, but if two targets are used simultaneously, $\mathbf{C}$ and $\mathbf{I}$ can be extracted and used as further corrections.

This analysis was explored by Tipton[11] and the author, but it was found that HERMES accpetance corrections for this technique are non-trivial and the study was not completed. This analysis may be ideally suited for the matrix method which handles acceptance corrections elegantly.

The large effect that fragmentation symmetry breaking may have on the "Δs" signal is motivation for a more precise determination of the fragmentation functions. For now, however, these effects can only be included as a systematic uncertainty.

4.3 Charge Dependance in the Acceptance

As described in Section 3.3.5, the strange sea polarization signal is proportional to the measured difference between the semi-inclusive pion and inclusive asymmetries. The measured asymmetries may, however, be affected by the HERMES acceptance, and this effect may cause the observed Δs signal.

For example, if the acceptance has a charge dependance and is larger for the negative pions than for positive ones,

$$\mathcal{A}^{\pi^-}(x, Q^2, z) > \mathcal{A}^{\pi^+}(x, Q^2, z) \tag{4.9}$$

then, the effective fragmentation functions will not obey the fragmentation symmetries, even if the theoretical functions do. Since the π^+ assymetry is larger than the π^- one, the total pion asymmetry is then expected to be suppressed, leading to a possibly false conclusion that

$$A_1^{\pi}(x) < A_1^{e^+}(x) \tag{4.10}$$

which is the observed signal from HERMES proton data. Thus, the positively polarized strange sea signal may be an artifact of the HERMES acceptance.

In general, however, the purity analysis does not support this hypothesis, since large positive Δs signal is observed when positive and negative hadrons are analyzed separately.

4.4 Positive Strange Sea

If the concerns of the previous two sections are put aside, the HERMES data and this analysis suggest that the strange quarks are strongly and positively polarized in the nucleon. This result contradicts the previous interpretations of inclusive DIS and hyperon decay analysis.

If this is indeed true, one feature remains unknown. Since the light quark sea is found to be largely unpolarized, in order to produce strongly polarized strange sea a dynamic mechanism capable of such production without affecting the light quarks must exist.

4.5 Polarized Glue

The extraction of the Δs signal relies on the differences between the light quark and strange quark fragmentation. Güllenstern *et al.*[4] have suggested that a similar effect may occur with gluons. In leading order QCD, the photon-gluon fusion precess contributes to both inclusive and semi-inclusive events. In the case of strict factorization, the gluon contributions to the two types of events are assumed to be equal. However, if there is a difference between the gluon contributions, then a noticeable asymmetry may result. For example, the HERMES high momentum transfer measurement of ΔG uses the fact that hadrons from gluonic events have a higher average momentum transfer than quark scattering events. If the HERMES acceptance is biased against the high momentum transfer events, then the ΔG contribution to semi-inclusive DIS would decrease[11].

However, this interpretation is very problematic as it may not be reasonable to apply leading order QCD to the gluonic events over the entire HERMES Q^2. It is also necessary to calculate the suppression of gluonic fragmentation in order to make the Güllenstern calculation, which may not be possible[11]. Also, since the strange sea signal remains even when only semi-inclusive data is used, there needs to be a process that distinguishes pions from other hadrons.

Chapter 5

Conclusions

The 1996 and 1997 HERMES polarized proton data have been analyzed using the pion branching fraction analysis. In the simplest interpretation, the results indicate a strongly positively polarized strange sea in the nucleon. This result is supported by the results of another analysis technique, the purity analysis, performed by Tipton[11].

Many uncertainties, however, remain. The pion branching analysis is very sensitive to the fragmentation functions. Incorrect fragmentation models may have a large effect on this analysis. Another uncertainty is a possible charge dependence in the HERMES acceptance. Such dependence would influence the result. Full understanding of these effects must be achieved before a clear physical result can be obtained.

A maximally positively polarized strange sea is an unexpected result. If true, it points to a dynamic process within the nucleon that is affecting only strange quarks. Better understanding of this result can improve our understanding of the small-scale structure of matter.

Bibliography

[1] J. D. Bjørken and E. A. Paschos. Inelastic electron-proton and γ-proton scattering and the structure of the nucleon. *Physal Review*, 185(5):1975+, 1969.

[2] Michael Düren. *The HERMES Experiment: From the Design to the First Results.* PhD thesis, Friedrich-Alexander-Universität Erlangen-Nürenberg, Den Naturwissenschaftlichen Fakultäten, July 1995.

[3] Leonid L. Frankfurt et al. The valence and strange-sea quark spin distributions in the nucleon from semi-inclusive deep inelastic lepton scattering. *Physics Letters B*, 230(2):141+, 1989.

[4] S. Güllenstern et. al. Semi-inclusive polarized lepton-nucleon scattering and the anomalous gluon contribution. *Physics Letters B*, 312:166+, 1993.

[5] Richard P. Feynman. Very high-energy collisions of hadrons. *Physics Review Letters*, 23(24):1415+, 1969.

[6] J. Stewart for HERMES Collaboration. The hermes polarized hydrogen internal gas target. In *Workshop on polarized targets and sources*, 1997.

[7] Phil Geiger. *Measurement of Fragmentation Functions at HERMES.* PhD dissertation, Ruprecht-Karls-Universitaet Heidelberg, Den Naturwissenschaftlichen Fakultäten, January 1998.

[8] Janusz M. Niczyporuk. Quark flavor tagging in polarized semi-inclusive deep inelastic scattering. Bs thesis, Massachusetts Institute of Technology, Department of Physics, June 1997.

[9] Dirk De Schepper. *Spin-dependent Deep Inelastic Positron Scattering from a Polarized Helium-3 Internal Gas Target.* PhD thesis, Massachusetts Institute of Technology, Department of Physics, June 1997.

[10] Dirk De Schepper and Art Mateos. Private Communication.

[11] Bryan Tipton and Felix Dashevskiy. Investigations of strange sea polarization in the hermes 96-97 data. HERMES Collaboration Internal Note 98-073, December 1998.

[12] Wolfgang Wander. *Reconstruction of High Energy Scattering Events in the HERMES Experiment.* PhD thesis, Friedrich-Alexander-Universität Erlangen-Nürenberg, Den Naturwissenschaftlichen Fakultäten, June 1997.